Gravity & Magnetic Surveys at Little Cottonwood Water Treatment Facility Final Report

Paul Gettings & Derrick Hasterok

March 7, 2003

1 Introduction

In early February 2003, the Little Cottonwood Water Treatment Plant (LCWTP) commissioned a detailed gravity and magnetic study of the LCWTP facility to complement a refraction seismic experiment. URS corporation handled the actual contracting, with a delivery date for results of 24 February 2003. The final report was due before 13 March 2003.

Paul Gettings and Derrick Hasterok, both from the University of Utah, designed the survey, took the measurements, and analyzed the resulting data. Students from an exploration seismology class assisted in data acquisition as part of their class. Supplemental analysis will also be conducted as a class project, although results will not be done until after the March 13 deadline.

Original data and copies of this report are available on the World Wide Web at *http://terra.gg.utah.edu/lcwtp*. All software, except GM-SYS, is free, and available on request to either Paul Gettings or Derrick Hasterok. GM-SYS is commercially produced by Northwest Geophysical Associates.

2 Survey Design

URS indicated that the major desired result is a determination of depth to the "R1" boundary across the site. This is interpreted to be the contact between unconsolidated and semi-consolidated fill in the valley. Estimates of the depth to R1, based on assumed fault geometries and drill records in the north part of Salt Lake Valley, were around 300 m. Given the short time-frame of the project, it was decided to minimize the number of stations while maintaining sufficient spatial resolution.

Based on the 1 km square size of the site, a nominal spacing of 64 m E-W and 70 m N-S was chosen for gravity and magnetic stations. Gravity and magnetic data would be acquired at each site in as short a time as possible. After masking

the grid for residential and inaccessible areas, a total of 83 possible stations were sited and marked.

Gravity data acquisition used a Scintrex CG-3M precision gravity meter in a field survey mode. Meter choice was dictated by availability rather than precision concerns; available LaCoste & Romberg G-series meters were not known to be in good condition for the survey. Gravity data were automatically recorded by the meter.

Magnetic data were acquired using a pair of Geometrics proton-precession magnetometers. One meter (model G-856) was setup as an automated base station near the center of the site, and left running during the field campaign. Readings at each station were taken with a model G-816 magnetometer, which was manually transcribed.

Station positions were kept as close as possible to the originally mapped locations, but final positions were obtained from RTK GPS data. Survey station P-18 (next to the new administration building on the site) was used as a local base. RTK GPS positions are precise to better than 10 cm vertically and 5-10 cm horizontally. Vertical accuracy was taken to be 10 cm for gravity processing.

3 Gravity Survey

3.1 Gravity Data Processing

Gravity data were reduced using standard USGS software for instrument drift, Earth tides, and terrain corrections. Instrument drift was computed using repeated occupations of survey station P-18 (near the administration building on the site); three occupations per field day (morning, lunch, and evening) were used to compute a 2-part linear drift function for each day. Additional readings were taken at the SLC AA absolute gravity station, and those readings used to compute observed gravity at the field stations. Instrument drifts were within expected values of 0.01 to 0.04 mGal/day.

Solid Earth tides were removed from the data using Tamura's harmonic formulation [3]. Station positions were taken from RTK GPS data, and time from the internal clock of the Scintrex gravimeter. Time values are accurate to better than 1 minute when compared to local time derived from the atomic clock time signals.

Terrain corrections for the gravity stations were computed using the USGS program *terrain_correct*, which uses a 15 arcsecond DEM to compute corrections to a radius of 167 km. Hand corrections were not applied to the data because the local topography of the site is generally gentle, and contains no large changes that are not captured in the DEM. Stations were situated to minimize possible terrain effects. Buildings and other structures have little effect on the gravity readings, due to the relatively small mass of a structure, and its position to the side of a meter. Stations taken over the water treatment tanks have not been corrected for depth of water in the tank; gravity effects of the tanks will appear in the data as an anomalously low region, which can be easily modeled,

if necessary.

Complete Bouguer gravity anomalies were computed for a variety of reduction densities between 2.0 and 2.67 g/cc. Due to the low relief of the survey area, and the relatively stable geology under the survey points, the choice of reduction density is nearly arbitrary; different reduction densities offset the entire survey, but do not change the peak-to-trough amplitude of anomalies, or anomaly shape. This was checked by comparing the magnitude of variation across the survey for different reduction densities. An example complete Bouguer gravity anomaly map is shown in figure 1, for a reduction density of 2.67 g/cc. Gravity stations data has been gridded (using cubic splines) and contoured onto a 100x100 cell grid to produce the map.

To allow use of the SEG North American gravity grid for regional removal, a reduction density of 2.67 g/cc was chosen for the interpretation. Regional gravity gradient was removed by linear interpolation of the SEG North American gravity grid. This is a 4 km gravity grid which provides a convenient low-pass filtered regional gradient. Closest grid points were interpolated to produce a regional gravity value at each station. Residual gravity values at each station were then gridded using a cubic spline algorithm to produce a uniformly spaced grid over the survey area. This grid contains 100 cells in each direction. A colored contour map of the residual grid is shown in figure 2.

3.2 Gravity Data Interpretation

The residual gravity clearly shows a linear trend from a gravity high in the east to a low in the west. This correlates well with the expected signal from the Wasatch fault, and is not well correlated with topography. Lack of correlation with the site topography indicates that the residual gravity anomaly is likely due to subsurface structure. In addition to the first-order linear trend, there is also secondary structure evident in the residual map. This is likely due to variations in the basement interface or basin fill. Quantitative estimates of depth to basement, or mapping of the sediment contacts, requires at least 2d modeling of cross-sections.

Due to the short time available for the project, 2d modeling was chosen to produce useful results rapidly. Models of three cross-sections, shown as E-W lines on figure 2, have been made using the software package GM-SYS. This package includes magnetic modeling capability, but this was not used since the magnetic data are of such poor quality.

Each model was hand-fit to the profile data, which is taken from the gridded gravity values. Each cross-section was fit individually, although coherence between the cross-sections is maintained at a coarse scale. Since the gravity modeling was done after the initial seismic results were available, the depth to the semi-/un-consolidated fill interface (R1) was initially fixed at sim90 m for all cross sections.

Density values for rock layers were taken from the well logs reported by Hill [1], and then differenced from the Bouguer reduction density of 2.67 g/cc. Hence, densities used in the models were -0.52 g/cc for unconsolidated fill, -0.47

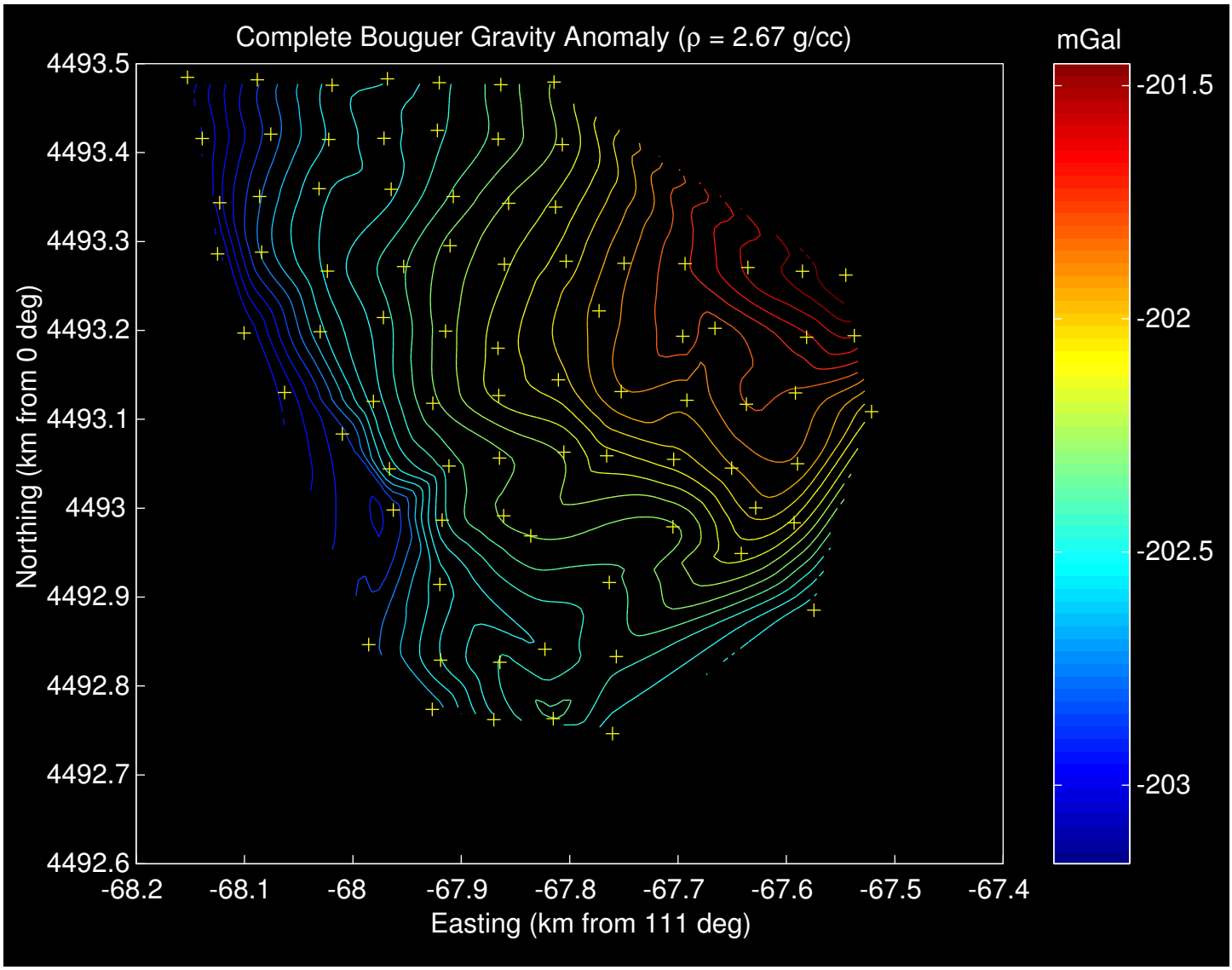

Figure 1: Contour map of complete Bouguer gravity anomaly. Reduction density is 2.67 g/cc. Yellow crosses indicate gravity and GPS stations. Note the dominant linear trend, and clear second-order structure. Contour interval is ∼0.08 mGal.

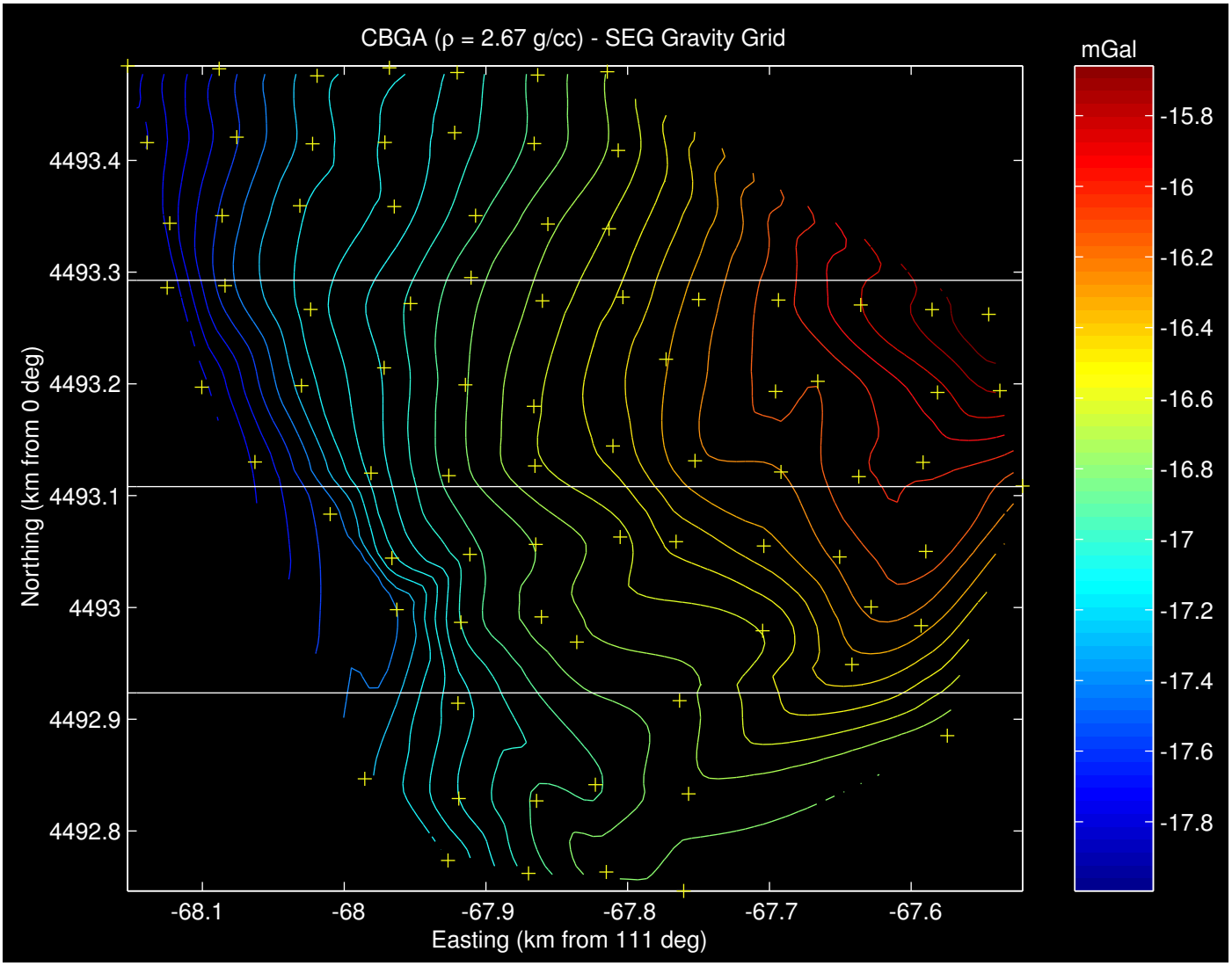

Figure 2: Contour map of Complete Bouguer Gravity Anomaly minus computed "regional" gravity anomaly from SEG gravity grid. Reduction density is 2.67 g/cc. Yellow crosses indicate gravity and GPS stations. Note the dominant linear trend, and clear second-order structure. White horizontal lines indicate 2d cross-sections for modeling. Contour interval is ∼0.08 mGal.

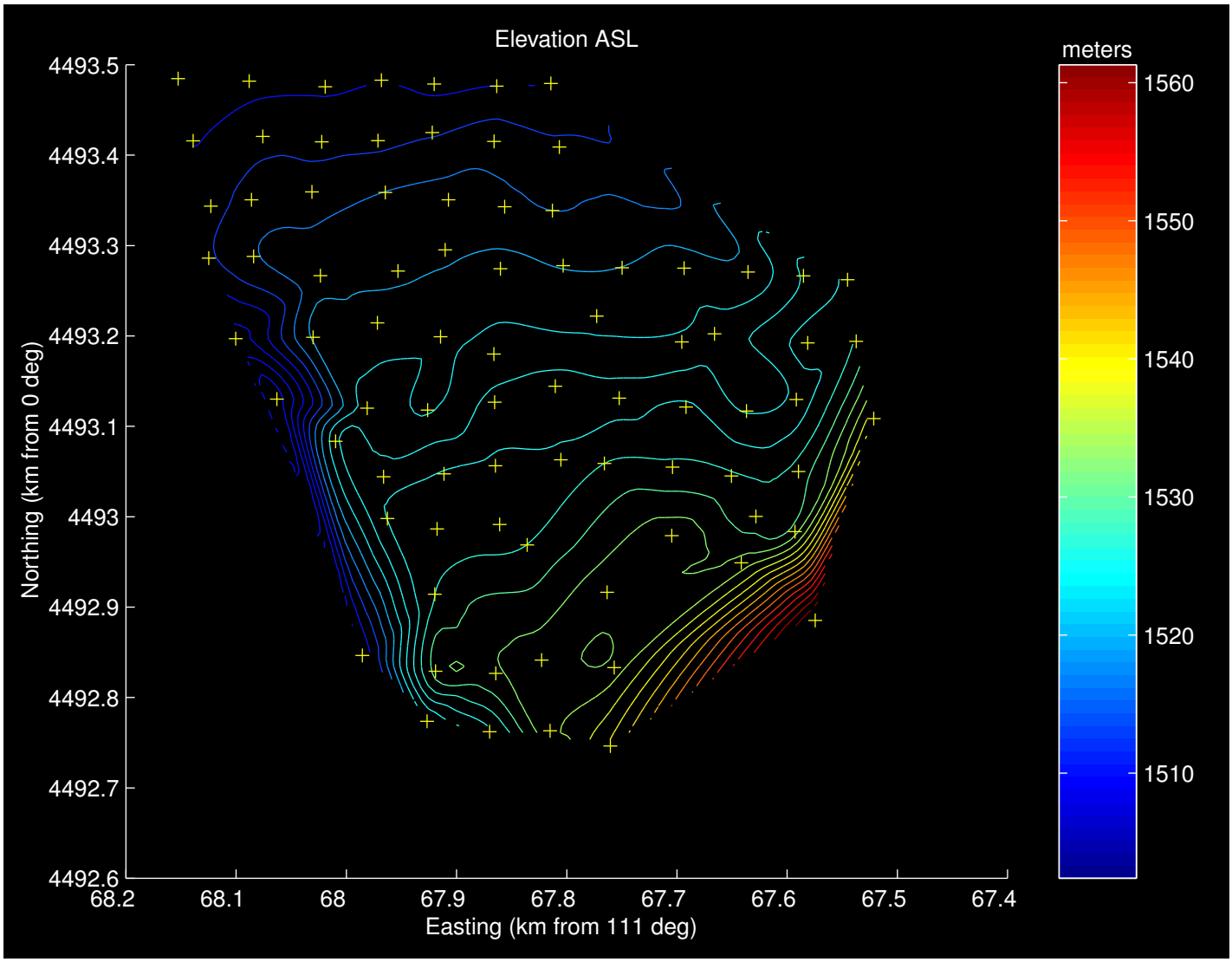

Figure 3: Contour map of site topography, made from RTK GPS elevations. The elevation of P-18 (the GPS base) was supplied by MWDSLS as 1520.63 m.

g/cc for semi-consolidated fill, 0.0 g/cc for basement, and -0.67 g/cc for near-surface fill (solids residuals, etc.). Each layer is assigned a constant density - there is no compaction model. Note that it is assumed that density changes in a model correspond to lithology changes, but this is not strictly required. Particularly in this study area, where the fill density contrast is small (-0.05 g/cc), gravity modeling results may not perfectly mimic lithology changes.

Model cross-sections are shown in figures 4, 5, and 6. These cross sections have 2 panels; one of an overall view of the model to basement, and a plot of the study region to emphasize near-surface density changes. All models use the same density values, so only geometry is varied among the cross-sections. An initial depth of 95 m is used for the R1 interface for all cross-sections. This depth is perturbed slightly along the profile to improve model fit to the data, where short-wavelength signals are seen.

Initial fitting of the gravity data is done through setting the angle of the Wasatch fault, which determines the overall angle of the gravity gradient. This first-order (dominant) structure in the data reflects the steeply dipping ($\sim 60°$) normal fault to the east of the site. The model is very sensitive to the angle and position of the fault, which was chosen to reach surface elevation $\sim$500-1000 m to the east of the eastern end of the profile. Fault angle was chosen to be $\sim 60°$ for all cross-sections, as this fits the overall trends best.

Since the seismic results indicate a depth to R1 of 95 m, the interface was initially set to $\sim$90 m depth, and the broad second-order structure in the gravity data fit using basement relief. The resulting basement relief shows a large, vaguely round, lump next to the fault under the site. This lump can be interpreted as a fault block bounded by the Wasatch and a secondary fault in the basin basement; a cartoon of this idea is shown in figure 7. More data, such as seismic reflection, are necessary to refine and confirm this interpretation.

Short-wavelength secondary structure in the data was fit using modifications to the geometry of R1. All cross sections show a double-peak structure in the R1 interface, with shallow minimum depths of 10 to 80 meters. Due to the nature of the anomalies, it is unlikely that the model results are reflecting very near-surface effects; stations near water tanks should show a short-wavelength gravity low, which would be modeled as a deepening of the R1 reflector and/or basement. The data show short-wavelength gravity highs, which indicate increased mass, and hence a shallowing of the basement and/or R1 reflector.

In fitting the cross-section models to the data, constraints were imposed on basement topography: no more than 1000 m of vertical change were allowed across the survey area in the basement. This is not much of a concern, since changes in the basement topography have broad effects in the computed gravity, and hence the short-wavelength structure cannot be fit with basement; it must be fit using changes in the R1 interface.

Note that the relatively large departure of the computed gravity at the western end of the profiles is a result of the modeling algorithm and far offset geometry, which has no noticeable impact on the survey area modeling. The interpretations do not include these areas, and so the misfit is ignored.

In cross section one (figure 4), note the very shallow depth of the -0.52 g/cc

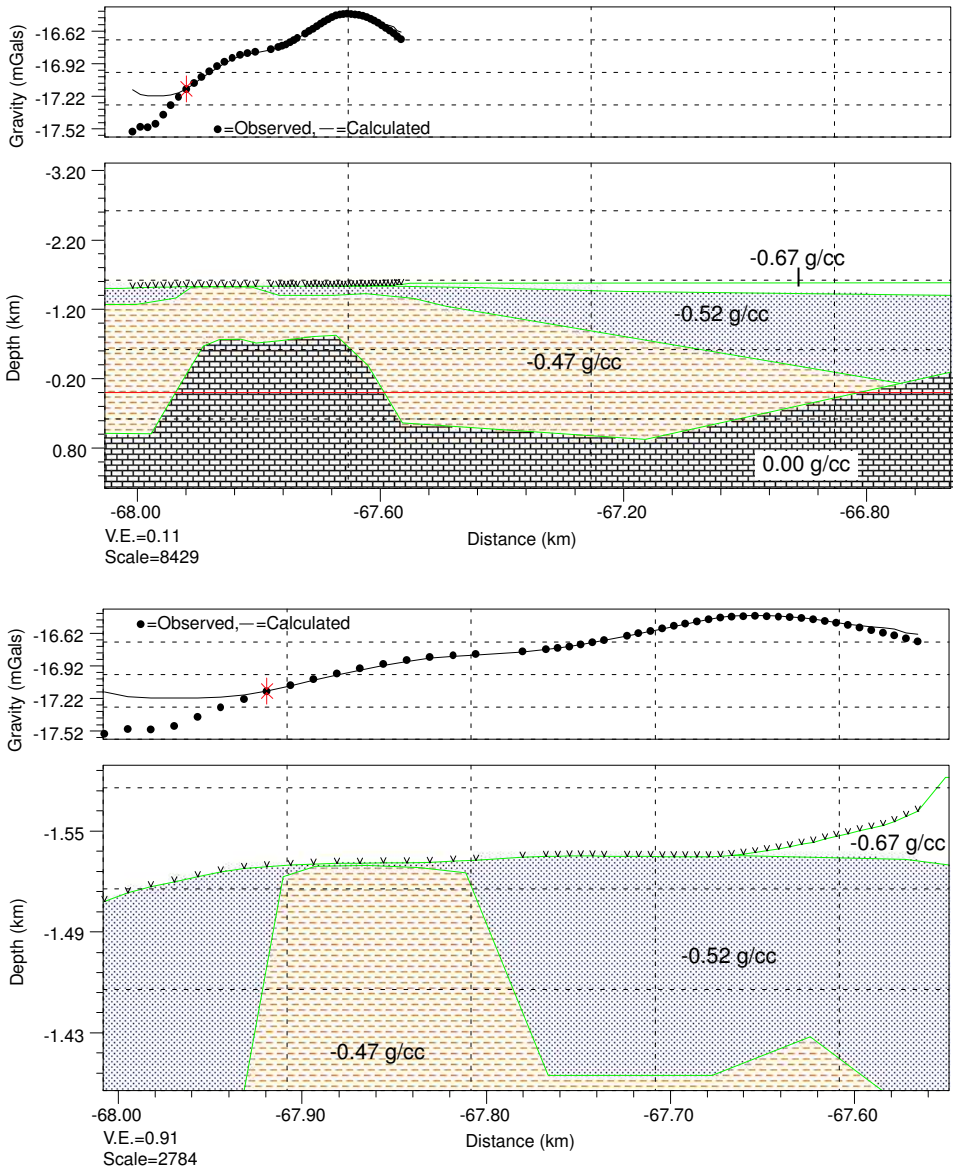

Figure 4: Cross section 1 - South. Modeled cross section in the southern part of the survey site. Upper panel shows overall model; lower panel is expanded view to highlight near-surface structure.

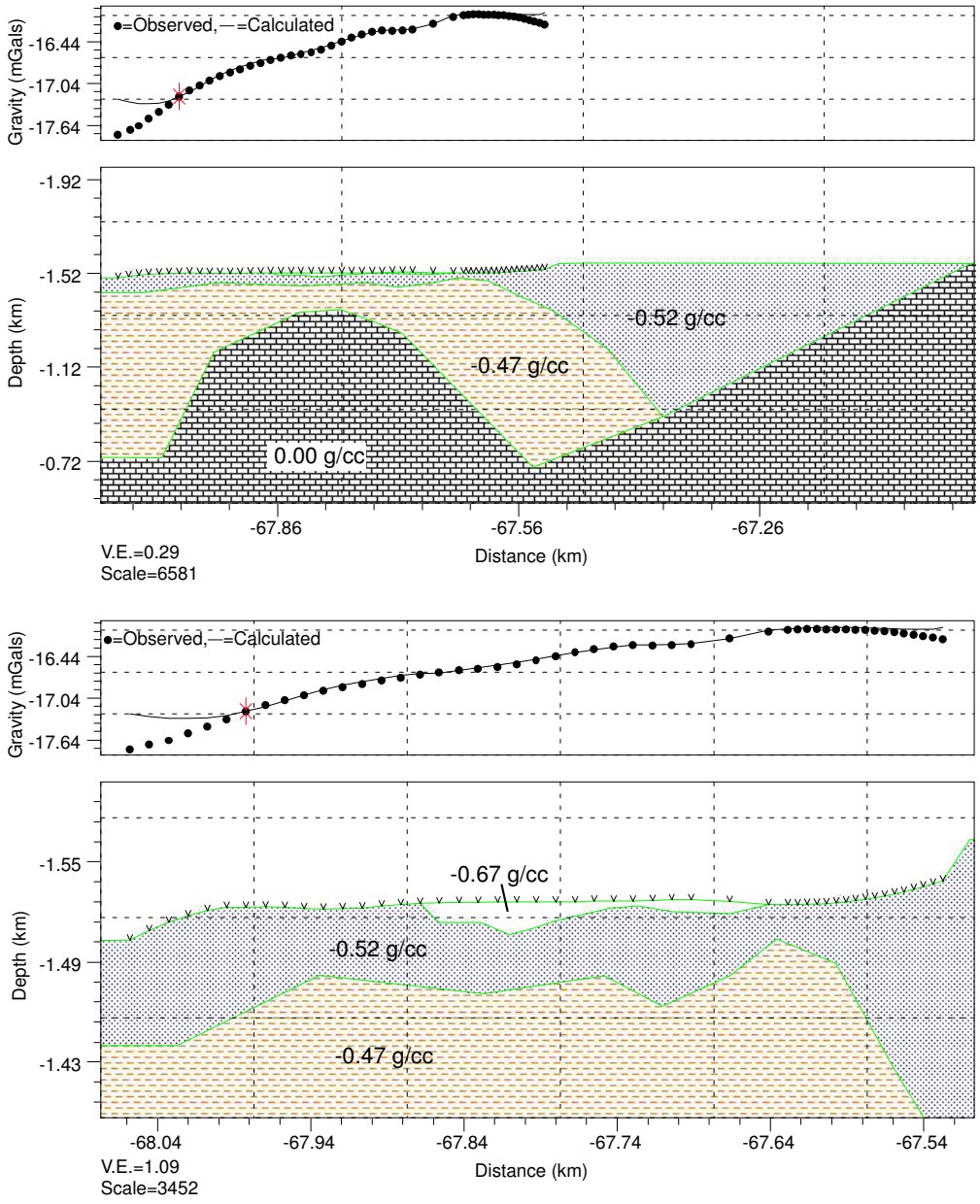

Figure 5: Cross section 2 - Center. Modeled cross section in the central part of the survey site. Upper panel shows overall model; lower panel is expanded view to highlight near-surface structure. Note the -0.67 g/cc trough in the center; this is most likely due to the close proximity of the sludge drying beds. Density contrast has been kept at -0.67 g/cc to make the trough more visible, although unrealistically thick.

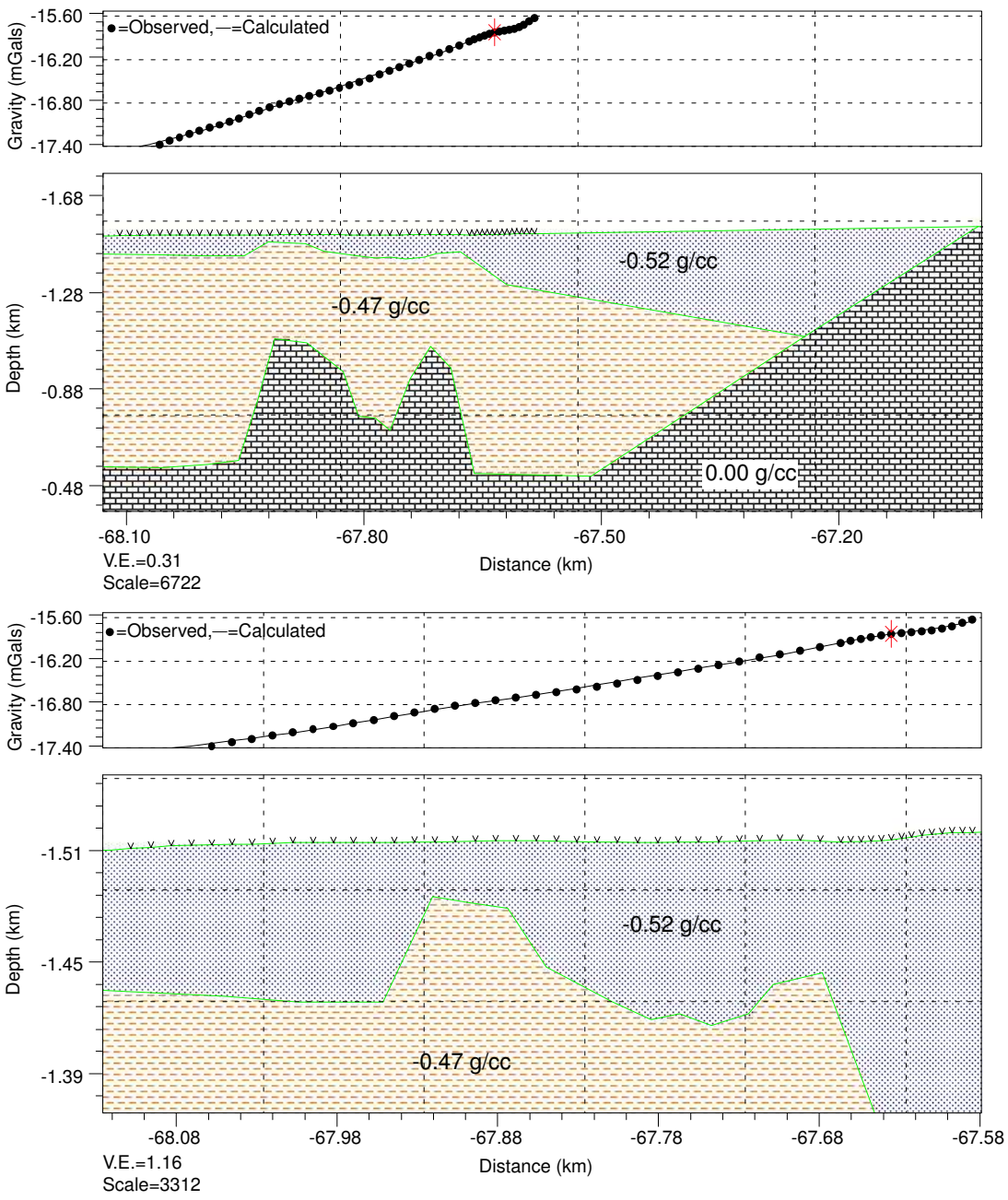

Figure 6: Cross section 3 - North. Modeled cross section in the northern part of the survey site. Upper panel shows overall model; lower panel is expanded view to highlight near-surface structure. This cross-section is closest to the seismic refraction line of Schuster [2].

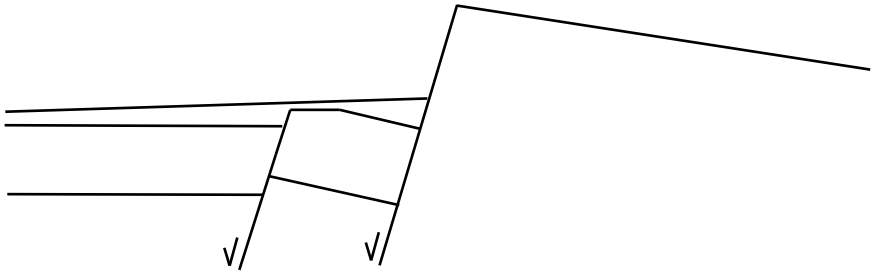

Figure 7: Cartoon of small fault block shown as basement high in gravity models. Note that the relatively poor sensitivity of the gravity to subtle geometry of the fault block means that a sharply defined block can be adequately modeled using a rounded block.

to -0.47 g/cc density change. This shallow depth, of <10 m in places, may be the result of local density variations, or may represent real structure. Without more data, preferably seismic reflection data, it is difficult to distinguish a real structural high from a local increase in the unconsolidated sediment density. Such a local shift could be do to either a slight change in sediment type, or the presence of an extensive dense mass in the near surface. As both buildings and water have lower densities than the near-surface fill, it is unlikely this gravity high is caused by a man-made structure under the profile. Also note the presence of a low-density body at the eastern edge. This body partially compensates for the lack of detailed topographic information to the east of the survey area; the modeling algorithm is incorrectly computing predicted gravity without the correct topography, despite the use of a topographic correction to the observed gravity values. This is to be expected, and the low density body brings the predicted gravity back into agreement with the observed values. However, the shape of the body should not be considered realistic beyond the edge of the survey area; the observed data do not sufficiently constrain the modeling.

Cross section two (figure 5) is near the sludge drying ponds, and hence the gravity models require a local low-density trough in the center of the profile. Note that the model uses a density of 2.0 g/cc (-0.67 g/cc relative to the Bouguer density), rather than the density of water or air (-1.67 or -2.67). This smaller density contrast increases the depth of the trough necessary to fit the data, which highlights the trough's existance. Using the density contrast for air, the trough would exist and be invisible in the plots. Interpretations of cross section two should take this fact into account.

Cross section three (figure 6) shows similar basement and near-surface structure to the other cross sections, although without the very shallow sediment change of cross section one, or the low density trough of section two. This cross section is closest to the refraction seismic experiment of Schuster [2], and hence should show the best agreement with the seismic results. The gravity model still shows a double peak pattern in the sediment contact, along with a pronounced double peak in the basement. However, over most of the profile, the depth to

the sediment contact is nearly 90 m, roughly equal to the seismic results.

Note that the gravity modeling only determines density at depth, not lithology at depth. Although the gravity models show very shallow depths to the -0.47/-0.52 g/cc contact, interpreting this as the depth to the R1 reflector could be misleading. Gravity is solely dependant on density and depth, and the R1 reflector represents a velocity change, not a significant density change. The density contrast between the semi- and un-consolidated fills is very small (-0.05 g/cc), and may be swamped by a local variation in the unconsolidated sediment layer. For this reason, it is advisable to use the seismic results for a more reliable depth to R1 estimate, and the gravity results for an initial representation of the depth to basement.

4 Magnetic Survey

4.1 Magnetic Data

Magnetic data was collected using a Geometrics G-816 on a 2-meter staff with a continuously recording base station using a Geometrics G-856 on a 2m aluminum range pole. Data were collected at locations corresponding to gravity stations at 76 sites. Fifteen stations were immediately rejected when 1 m horizontal gradients exceeded 20 nT/m or had wildly varying values at a single location. These effects appeared to correlate with regions with high cultural noise near the station; i.e. power lines, ferrous scrap metals, locations of pipelines, etc.

4.2 Magnetic Data Processing

The remaining 61 stations were reduced to a common datum using base station time series to filter out effects due to diurnal variations and possible interference from magnetic storms. Figure 8 shows 61 stations passing the initial rejection test. The strongest gradients resulted in this figure from structures in the southern portion of the property, i.e. the filter building, classifier tanks, power substation, etc.

Data that appear affected by these structures were removed and the map re-gridded with 37 stations as shown in Figure 9. Figure 9 shows an increase in the total field to the northwest possibly resulting from the sludge drying beds; however, the region containing this large gradient is constrained by very few stations. A strong positive anomaly appears on the western edge of the property as a result of edge effects from the nearby steep topography. In the field in the northwestern section of the field area, anomalies have an approximate range of 60 nT. However, most anomalies are constrained by one measurement and therefore are likely due to near surface sources.

4.3 Magnetic Data Interpretation

Because of the high cultural nose on site and near surface anomalies affecting most stations, magnetic data give a very poor assessment of the basement/basin

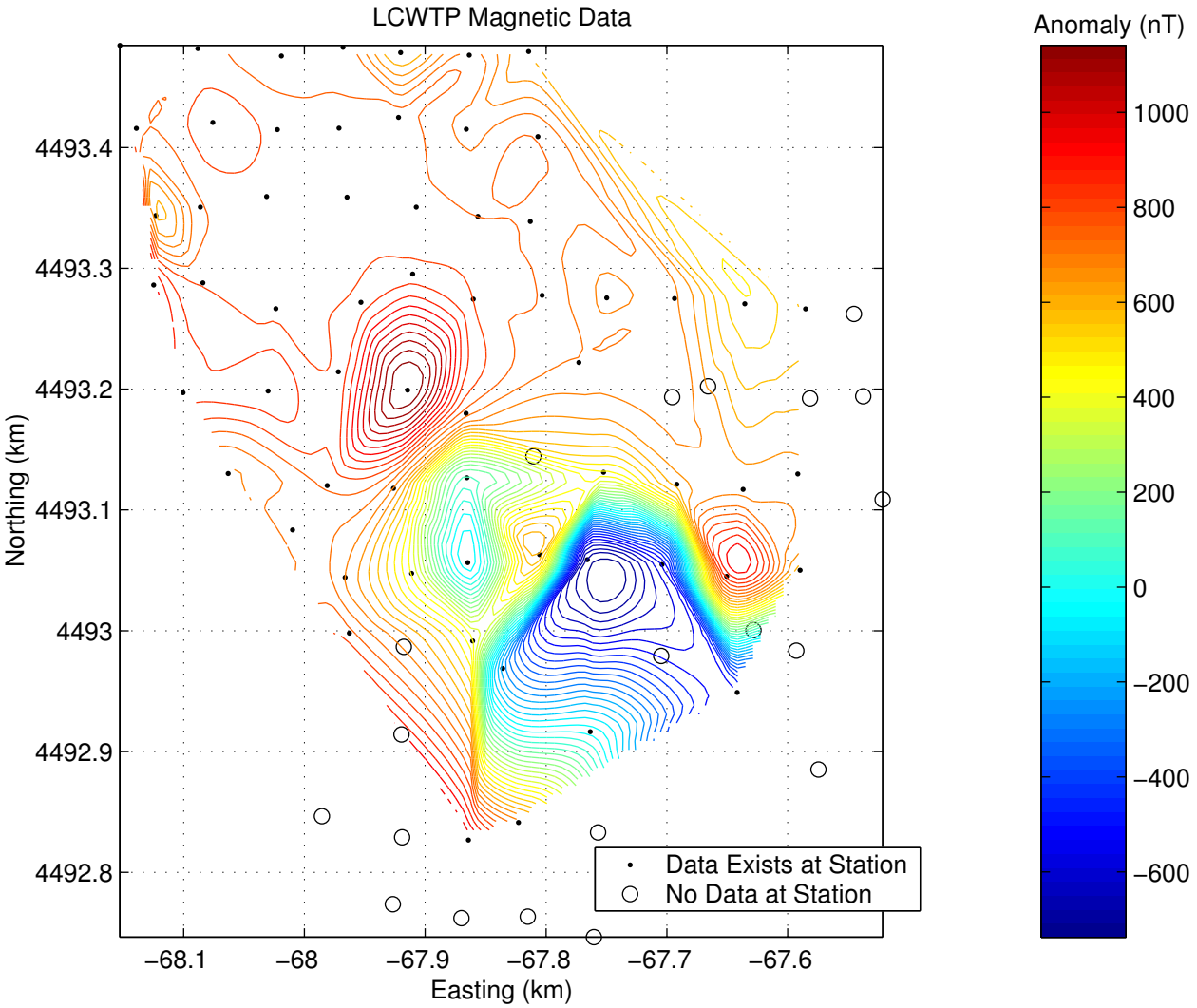

Figure 8: Colored contour map of magnetic data. Gravity stations with no or rejected data are shown as open circles. Contour interval is 12 nT. Data have not been referenced to IGRF.

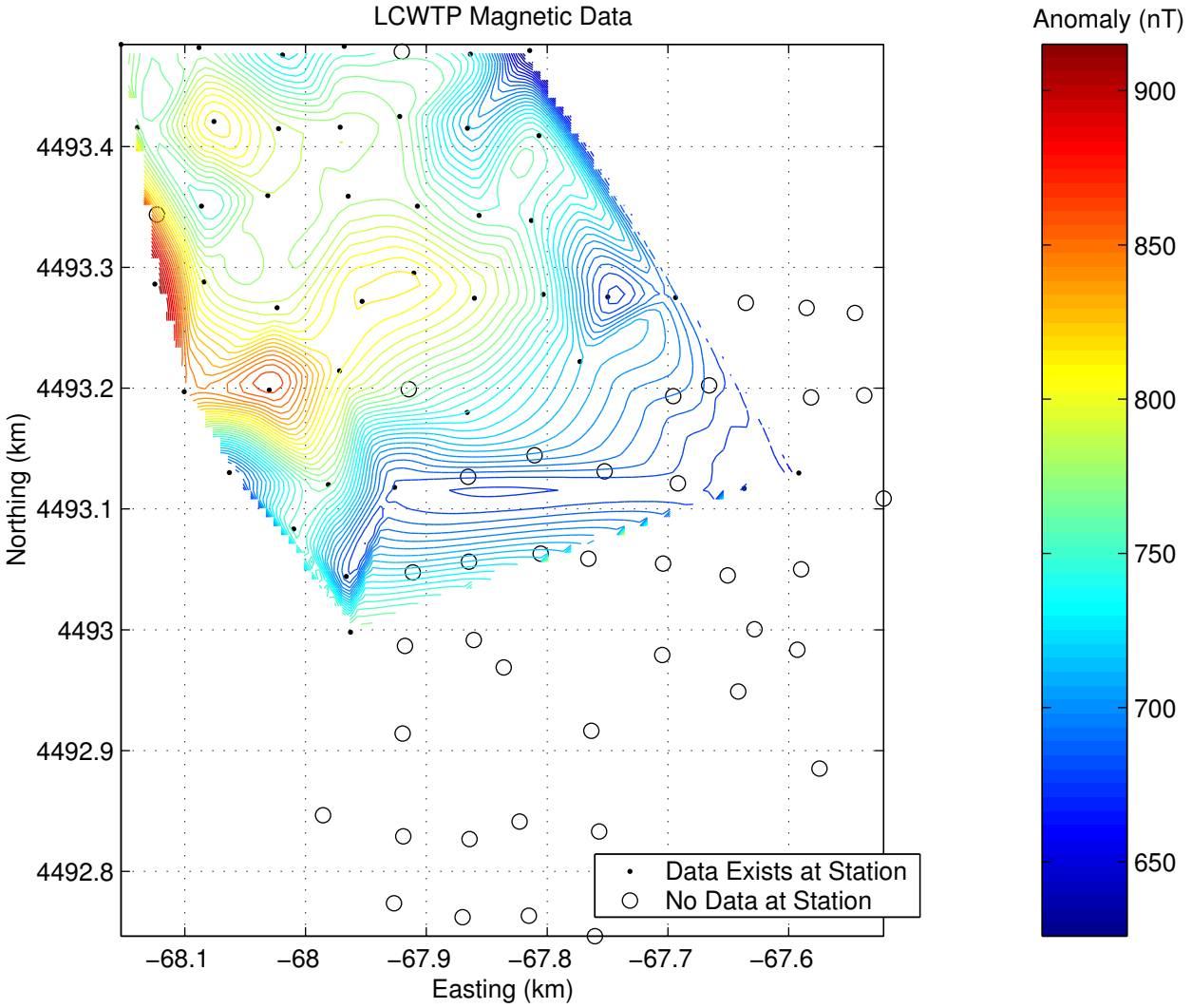

Figure 9: Colored contour map of magnetic data subset. Data with known cultural noise have been removed, and the remaining stations replotted. Stations without data in the contouring are shown as open circles. Contour interval is 10 nT.

interface. Therefore, no attempt has been made to include the magnetic data in the gravity interpretation.

5 Conclusions

Modeling of the gravity data, constrained with seismic results for the initial placement of the R1 interface and external structural knowledge of the Wasatch fault, produces reasonable cross sections across the study area. These cross sections show a consistent basement high under the study area, next to the Wasatch fault. This basement high is likely a fault block, although seismic reflection or (clean) magentic data is needed to confirm this interpretation.

Near-surface modeling results show very shallow depths for the semi- to unconsolidated fill contact. However, these shallow depths may represent local increases in fill density, rather than a lithologic contact or the R1 reflector. The low density contrast between the two fill types makes accurate determination of the R1 reflector difficult with only gravity data.

The lack of useful magnetic data, due to the extensive cultural noise, hampers the interpretation of the gravity data, but does not preclude obtaining useful results.

References

[1] Julie Hill. A finite-difference simulation of seismic wave propogation and resonance in the Salt Lake Valley, Utah. Master's thesis, University of Utah, 1988.

[2] Gerald Schuster. Forward-reverse refraction survey at Metropolitan Water Plant, 2003.

[3] Yoshiaki Tamura. A harmonic development of the tide-generating potential. *Bulletins d'Informations Marees Terrestres*, 99:6813–6855, 1987.